Analysis of 3 years of data from the gravitational wave detectors EXPLORER and NAUTILUS

P. Astone,[1] M. Bassan,[2,*] E. Coccia,[2] S. D'Antonio,[2] V. Fafone,[2] G. Giordano,[3] A. Marini,[3] Y. Minenkov,[2] I. Modena,[2] A. Moleti,[2] G. V. Pallottino,[1] G. Pizzella,[3] A. Rocchi,[2] F. Ronga,[3] R. Terenzi,[4] and M. Visco[4]

[1]*Sapienza University of Rome and INFN, Sezione di Roma, P.le A.Moro 1, 00185 Roma, Italy*
[2]*University of Rome "Tor Vergata" and INFN, Sezione Roma Tor Vergata, Via della Ricerca Scientifica 1, 00133 Roma, Italy*
[3]*Laboratori Nazionali di Frascati INFN, Via E.Fermi 40, 00044 Frascati, Italy*
[4]*IAPS-INAF and INFN, Sezione Roma Tor Vergata, Via del Fosso Del Cavaliere 100, 00133 Roma, Italy*

(Received 14 January 2013; published 23 April 2013)

We performed a search for short gravitational wave bursts using about 3 years of data of the resonant bar detectors Nautilus and Explorer. Two types of analysis were performed: a search for coincidences with a low background of accidentals (0.1 over the entire period), and the calculation of upper limits on the rate of gravitational wave bursts. Here we give a detailed account of the methodology and we report the results: a null search for coincident events and an upper limit that improves over all previous limits from resonant antennas, and is competitive, in the range $h_{\mathrm{rss}} \sim 10^{-19}$, with limits from interferometric detectors. Some new methodological features are introduced that have proven successful in the upper limits evaluation.

DOI: 10.1103/PhysRevD.87.082002 PACS numbers: 04.80.Nn, 95.30.Sf, 95.85.Sz

I. INTRODUCTION

In the quest for gravitational waves (GWs), a primary role among the possible sources has always been played by those astrophysical events that are expected to produce GW bursts, such as the gravitational collapse of stars or the final few orbits and the subsequent coalescence of a close binary system of neutron stars or black holes. The search for such transient GW requires the use of a network of detectors. In fact, the analysis of simultaneous data from more detectors at different sites allows an efficient rejection of the spurious outliers, either caused by transient local disturbances or by the intrinsic noise of the detectors. Resonant GW detectors have operated for decades in several laboratories around the world, reliably staying on the air for long periods with high duty cycle [1–3], mainly looking for burst events. The coming of age of laser interferometer detectors [4], with much better sensitivity and bandwidth, has led to a gradual phasing out of many resonant detectors.

The ROG Collaboration has built and operated two cryogenic, resonant-mass detectors, EXPLORER [5–7] at CERN and NAUTILUS [8,9] at the INFN Frascati National Labs (Italy). Both detectors have been on the air since the early 1990s, performing various joint coincidence searches [10–12]. In the period May 5, 2005 to April 15, 2007 they took part in the IGEC2 network [2,3] that collected and exchanged data, together with the Auriga detector at the INFN Legnaro National Labs (Italy) [13] and with the Allegro detector at LSU (USA) [14]. After that period, Allegro was shut down and data have been collected by the three surviving antennas, but never analyzed before.

All these detectors use the same principles of operation. The GW excites the odd longitudinal modes of the cylindrical bar, which is cooled to cryogenic temperatures to reduce the thermal noise and is isolated from seismic and acoustic disturbances. Both Explorer and Nautilus consist of a large aluminum alloy cylinder (3 m long, 0.6 m diameter) suspended in vacuum by a cable around its central section and cooled to about 2 K by means of a superfluid helium bath. To record the vibrations of the bar first longitudinal mode, an auxiliary mechanical resonator tuned to the same frequency is bolted on one bar end face. This resonator is part of a capacitive electromechanical transducer that produces an electrical ac current that is proportional to the displacement between the secondary resonator and the bar end face. Such current is then amplified by means of a dcSQUID superconductive device. Nautilus is also equipped with a dilution refrigerator that enables operations at 0.1 K, further reducing the thermal noise. In the period considered, however, the refrigerator was not operational, in order to maximize the detector duty cycle. Both detectors are equipped with cosmic ray telescopes, to veto excitations due to large showers [15–17]. The two telescopes rely on different technologies (scintillators for Explorer, streamer tubes for Nautilus) but both provide a monitor of comparable effectiveness and a continuous check of the antenna sensitivity [18,19].

At present, while the large interferometers VIRGO and LIGO are undergoing massive overhauls to upgrade their sensitivity, there still are two resonant detectors, Nautilus and Auriga, that continue to operate in "astro-watch" mode, i.e., as sentinels recording data that could be analyzed in conjunction with a significant astrophysical trigger, such as the explosion of a nearby supernova, or any astronomical event thought to be a possible source of GW.

We report here a study on three years of data from Explorer and Nautilus, starting from the end of the IGEC2 network, April 16, 2007 and stretching till June

*Corresponding author.
massimo.bassan@roma2.infn.it

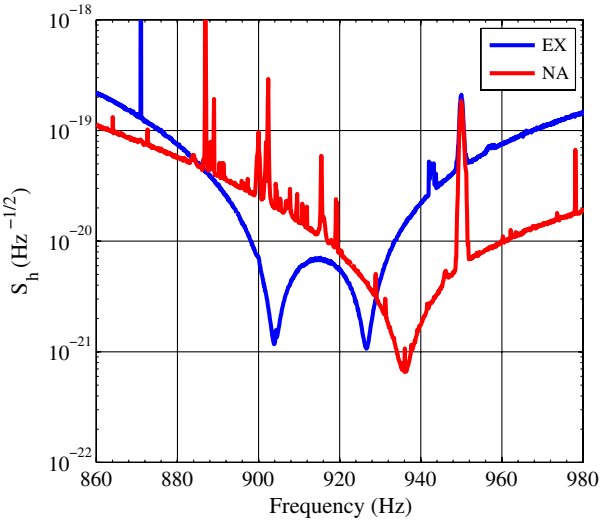

FIG. 1 (color online). Spectral sensitivity curves of EXPLORER and NAUTILUS. The two bandwidths overlap for a large fraction of the total sensitive region.

10, 2010, when Explorer ceased operations. The spectral sensitivity of the two detectors is shown in Fig. 1.

The purpose of this paper is to describe a search for short burst coincident events in the 3 years of data. The main interest of this analysis lies in several novelties that were implemented in the data analysis procedure and that are here detailed; namely, the construction of Receiver Operating Characteristics (ROCs) for the 2-detector observatory, in addition to the ones for each antenna, the optimization of the threshold pairs in order to maximize the detection efficiency, given an *a priori* choice of the background of accidental coincidences and an optimized procedure for the calculations of upper limits on the rate of GW bursts. The search was carried out keeping a low level of accidental coincidences, that we set at 0.1 over the entire period. Along with this search, we also performed a calculation of the upper limit (UL) on the rate of delta-like GW pulses impinging on the Earth. The method here described presents relevant improvements with respect to previously published searches performed with resonant detectors: we have used software injections of known signals to measure the efficiency of detection for each antenna and for the combined observatory. Based on the efficiencies so evaluated, and on the measured rate of accidentals, the analysis parameters were separately optimized for the coincidence search and for the UL evaluation.

Throughout this paper, we shall call ''events'' or ''outliers'' those data points in the filtered data stream that are larger than a given threshold: these points are selected by an automatic event finder procedure and constitute the database for our analysis.

The paper is organized as follows: in Sec. II we describe the data collected in these 3 years, the filtering procedure, the criteria chosen to segment the total observation period in 5 subperiods and the vetos applied to both data and events. In Sec. III the procedures of software injection and time-delayed coincidences are detailed. The detectors are characterized in terms of efficiency and accidentals in the various time segments and the ROCs are generated, both for the individual antennas and for the combined observatory; on the basis of these parameters, in Sec. IV the thresholds for the ''true'' (zero-delay, on time) coincidence search are chosen and the search is performed. Finally, in Sec. V, we describe the procedure used to compute the upper limit for the flux of GW radiation. This procedure, quite different from those used in the past, is optimized in each of the subperiods and for each of the amplitudes of GW signals considered.

Some final considerations conclude the paper.

II. THE DATA

Data are collected by the two detectors with almost identical hardware and software. The output of the SQUID amplifier is conditioned by band pass filtering and by an anti-aliasing low-pass filter, then sampled at 5 kHz and stored on disk. Sampling is triggered by a GPS disciplined rubidium oscillator, also providing the time stamp for the acquired data.

The data are processed off-line, applying an adaptive, frequency domain filter matched to delta signals. The noise characteristics estimate is updated using data averaged over 10 minutes periods. The signal response is computed using a model for the detector, fitted with the measured values of frequencies and decay times of the system resonances. Both the model and the signal response were validated by hardware injections of known signals: the filtered output matched the expected value to better than 10%.

The filtered output of the detector is a time series normalized so to express the instantaneous dimensionless wave amplitude $h(t)$. The filter is designed and optimized for delta-like signals, but it works equally well [20] for a wider class of short bursts, like e.g., damped sinusoids with decay time $\tau < 5$ ms.

Although the detectors produce quite stationary data, their characteristics did change a few times over such a long observation period: in some instances, these differences were due to actual changes in hardware (e.g., substitution of a preamplifier), other times to some non identified factors. We found it useful, to the purpose of the study detailed below, to segment the analysis in different periods where both detectors had noise behavior (average noise energy) [21] consistently stable, within the statistical fluctuations. This allows us to better optimize the search in each period. Consequently, we identified 5 time stretches (see Table I), that roughly coincide with solar years, and ran separate optimized analysis on each subperiod. Stretch #2, the end of 2007, covers a short period, when Nautilus operations were badly disturbed: we shall show that the adopted procedures automatically

TABLE I. The time stretches $T_i (i = 1 \ldots 5)$ used to run different optimization in our analysis. $\sqrt{\langle h^2(t) \rangle}$ is the long term average of the amplitude noise.

Subperiod T_i	Begin-End	Days of good data	$\sqrt{\langle h^2 \rangle} \times 10^{-19}$ Explorer	Nautilus
#1 : 2007 A	Apr. 16–Dec. 5	162	4.57	3.47
#2 : 2007 B	Dec. 6–Dec. 31	12	4.21	5.04
#3 : 2008	Jan. 1–Dec. 31	232	4.43	4.36
#4 : 2009	Jan. 1–Dec. 31	242	3.82	2.52
#5 : 2010	Jan. 1–Jun. 10	113	3.98	2.39

minimize the contributions from bad periods both for the coincidence search and for the upper limit evaluation.

Before we start describing the procedure, two comments are in order:

(1) when segmenting the data in subperiods to be treated separately, or to run separate optimizations of the search parameters, we must ensure that each subperiod be long enough to provide a sufficient statistics, and in particular to avoid that any particular outlier or temporary noise affect in a sizable way the final choices. We found that a few days of data is somehow the minimum duration for this purpose;

(2) if the procedure is properly devised, the addition of any information or data set, however poor its quality with respect to the rest of the data, should not reduce the quality of the total result. On the contrary, a correct way of putting together all the information can only produce a better result.

A. Data selection

The data were selected with different cuts, applied both to the data stream and to the list of outliers. All criteria, studied in the past and in use for several years, were a priori chosen and blindly applied. The vetos that cause elimination of entire periods of data stream include:

(i) when acquisition flags or operator's notes are recorded, indicating bad or suspected periods (e.g., cryogenic refills, activity around the detector . . ..)

(ii) when the noise of the filtered data, averaged over 10 minutes, rises above a given value (about 5 times the long term average)

(iii) when the reference tone, a monochromatic signal monitoring the gain of the electronic chain, falls outside a given range

(iv) when an excessive amount of wide-band noise is present. Wide-band noise, usually of electronics origin, is monitored on two frequency bands, above and below the useful bandwidth of the detector.

(v) when auxiliary channels exhibit mean values above predetermined levels. Auxiliary (or veto) channels include seismic monitors, SQUID locking working point, nitrogen (on Explorer) and helium flow and more.

These cuts reduce the amount of available data for the coincidence analysis to 761 days, i.e., two thirds of the 1152 days of total observation period. The main contribution to these cuts is due to operations of cryogenic maintenance (liquid helium refills) that we chose to perform in different times on the two detectors, so that at least one were always operational.

On these data, an automatic event finder procedure selects the "outliers." All data points remaining above a chosen threshold are grouped in one *event*. An event can extend over more than one group if the signal falls below threshold for a time shorter than the *dead time*, set to 1 s. For the class of short signals discussed above, the shape of

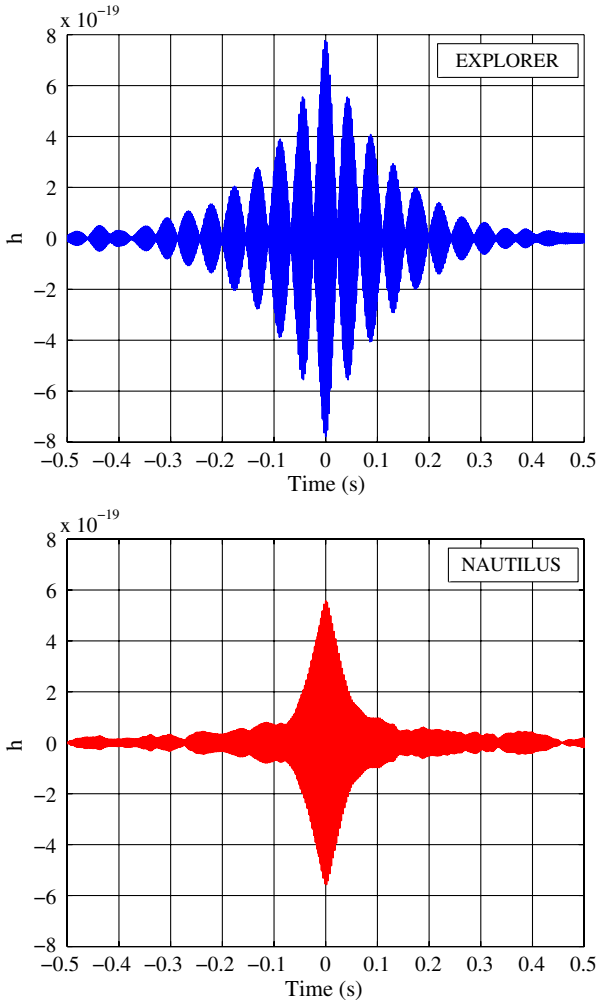

FIG. 2 (color online). Excitation of the detectors, as seen in the filtered data, due to two large cosmic-ray showers: an event of Explorer 2008 and an event of Nautilus 2007. Only the maximum value of these signals can be interpreted in terms of the assumed $h_{\rm rss}$ excitation; the shape of the pulse is due to the antenna response. The two plots are so dissimilar because of the differences in the bandwidths (see Fig. 1): while Nautilus has its sensitivity around one main frequency, Explorer is most sensitive on two frequencies and therefore its time-domain response exhibits beats.

the event is mostly due to the antenna response function (see, e.g., Fig. 2). Each event is then characterized by the amplitude $h_{\max}$ and time of the largest sample; the relation between the peak output value $h_{\max}$ and the input signal *root sum square amplitude* $h_{\rm rss}$ is simply assumed to be $h_{\rm rss} = h_{\max}\sqrt{\tau}$, where we chose, as usually done for resonant detectors [22], $\tau = 1$ ms. Further characteristic are recorded for each event, such as: starting time, total time length, integrated amplitude of the samples above threshold, average noise before the event. We set for this selection a threshold at critical ratio CR $= 5$ with respect to the average noise level, continuously updated.

A further selection was then applied to the outliers, in order to implement other cuts:

(i) an event should remain above threshold for a time consistent with its amplitude (the decay time for the filtered data is the inverse of the detector bandwidth).

(ii) cosmic ray showers are known to produce short bursts of excitation in the antennas. The events must not be in coincidence with a shower, as recorded by detectors installed above and below both antennas [16,17].

These two selections veto a very small fraction of the events, usually less than 0.1%.

III. DETECTORS CHARACTERIZATION

In order to perform a "fair" search for coincidence, all "human handles," i.e., adjustable parameters, must be *a priori* set before starting the search. To this purpose, we have applied a very large number of software injected events to determine the efficiency of both detectors to short bursts of GW. Likewise, the background of accidental coincidences is determined via a large number of time shifts. For a given level of accidentals, *a priori* set, the efficiency is then maximized with a proper choice of the thresholds. Only at this point, we can "open the box," i.e., look at the zero delay coincidences and assess its significance. The following subsections give some details about this characterization procedure.

A. Accidentals

The evaluation of the expected background of accidental coincidence was performed with the usual method of the time shifts. The lists of events, one for each detector, extracted from the data as described in Sec. II, were compared after shifting the time stamp of one of them. The event times of one detector were delayed, with respect to the other ones, 10,000 times in steps of 1.5 seconds (i.e., between $\pm 7,500$ s, excluding the zero time shift). This value is larger than the dead time [20] inserted by the event finder. The search of coincidences in each of the 10,000 cases, performed with a time window of 15 ms as discussed in Sec. III C, produces the data base of unphysical coincidences from which we learned the background characteristics. Table II summarizes the results.

TABLE II. Accidental (time-shifted) coincidences ($N_{\rm acc}$) in the 5 subperiods analyzed, obtained with the lowest threshold, $h_{\rm rss} = 3.56 \times 10^{-20}$ s$^{1/2}$, used in this analysis.

Subperiod	Duration (*day*)	$N_{\rm acc}$ *in* 10^4 *shifts*	$\bar{N}_{\rm acc}$/(day · shift)
#1 : 2007 A	162	5,635,671	3.48
#2 : 2007 B	12	640,143	5.33
#3 : 2008	232	6,667,062	2.87
#4 : 2009	242	3,061,314	1.26
#5 : 2010	113	1,042,858	0.92

B. Software injections

Large sets of software injections were performed in order to determine the efficiency of the detectors to delta-like signals of different amplitudes. As mentioned above, the extensive cosmic ray showers excite the bars, closely approaching the effect of a short GW burst. We took advantage of this feature and used real signals, observed in coincidence with some particularly intense cosmic ray shower, as the prototype signal to be used for software injections (see Fig. 2 for an example of the signals applied). These signals, actually oversampled at 50 kHz, were scaled to the appropriate values of amplitude and added to the filtered data of each detector. This technique is much faster than that generally used, where one first generates the h-reconstructed data stream, then adds the injections to this stream and finally refilters and searches for the events. We validated our method by applying both techniques to a one-day sample of data, finding a very good agreement. The times of the injections were pseudo random, because we avoided injections too close to the beginning or end of each period of good data, and required a minimum distance of 10 seconds between two adjacent injections. Moreover, we added a delay, randomly chosen in the $[-2.3, 2.3]$ ms interval to the injection time of Explorer, to simulate the time of flight of a possible GW signal of unknown direction.

We injected signals of 10 different amplitudes, in the range of $h_{\rm rss}[7.97 \div 12.6] \times 10^{-20}$ s$^{1/2}$, at a rate of about 90 injections per day.

C. Efficiency

The usual event finder routine was then applied to the data containing the injected signals. For each subperiod and for each level of injected signal, efficiency charts were produced, displaying the percentage of detected signals with amplitude exceeding any given value. Figure 3 is a sample of such charts, showing the efficiencies in the subperiod 2009 for each antenna.

The injections also allow us to determine the time response of the detectors, and guided us in choosing the best coincidence time window to be applied. We found that a coincidence window of ± 15 ms assures an efficiency very

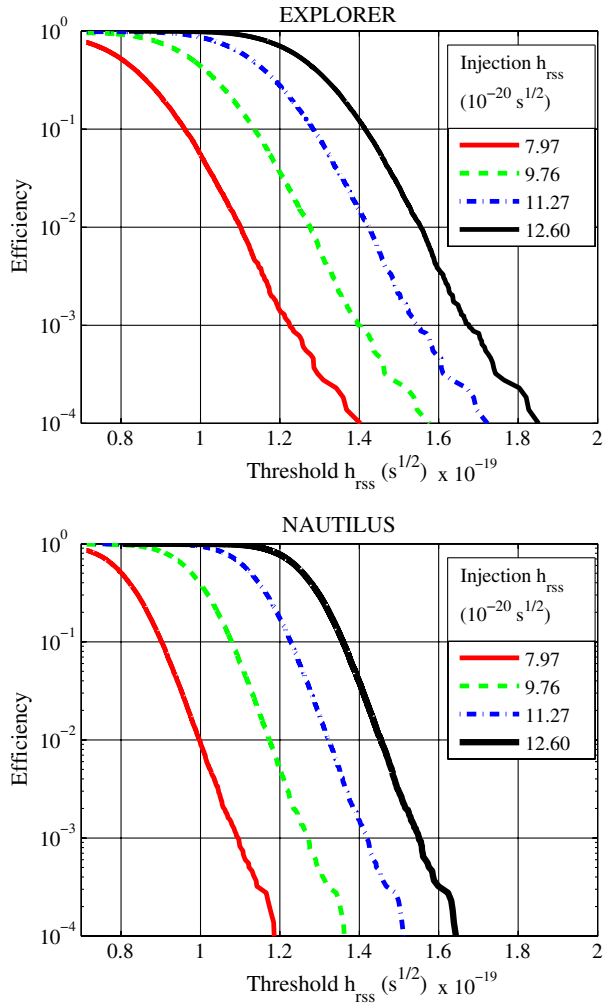

FIG. 3 (color online). Efficiencies of Explorer and Nautilus in 2009. The four lines refer to injections with $h_{\rm rss} = (7.97, 9.76, 11.27, 12.6) \times 10^{-20}$ s$^{1/2}$.

close to 1 for delta-like signals, even at the lowest injected amplitude: indeed, the measured probability of missing a coincident event with the chosen window of 15 ms is less than 1×10^{-4}. Besides, the chosen window is sufficiently wide to also accommodate, without significant losses of efficiency, other classes of signals [20] for which the detectors time response might be different.

D. Receiver operating characteristics

Efficiency and accidentals vs threshold amplitude completely characterize a detector. These two classes of information can be summarized in the Receiver Operating Characteristics or ROC.

It is worthwhile, in view of what follows, to briefly recall the procedure to generate a ROC: for each injected amplitude we sweep the threshold amplitude and we look up both the efficiency and the rate (or the total number) of accidentals. By eliminating the threshold value between these two relations, we derive a curve [efficiency vs event rate], that constitutes the ROC for that given signal amplitude.

In Fig. 4 we show an example of ROCs, for both Explorer and Nautilus, relative to year 2010.

It is to be remarked that, despite the fact that the detector hardware was virtually unmodified in all subperiods, the ROCs do vary, especially for Nautilus, from one subperiod to another (see Fig. 5).

As we are interested in the operation of both antennas as one detector, we can extend the concept of ROC to a coincidence search. In this case, in order to vary efficiency or accidental rate, we can act on either threshold, so that there exists an infinity of threshold pairs that can provide the same characteristics: we could have therefore infinite ROC curves for the same signal amplitude. However, keeping in mind that our aim is to maximize the efficiency of detection for a given accidental rate, we can focus our search on finding the pair of thresholds that gives the best efficiency for each value of accidentals. The ROCs for the Explorer + Nautilus compound observatory are therefore obtained with the following procedure:

(i) We choose a set of M threshold values and we sift through our data with a matrix of M*M thresholds: both in the list of events found with the injections

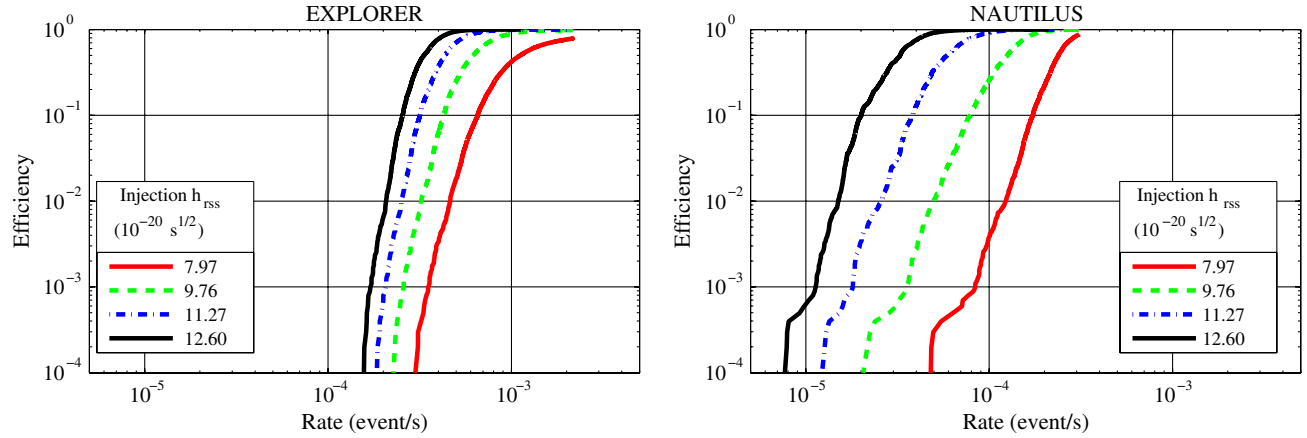

FIG. 4 (color online). ROCs for Explorer and Nautilus in year 2010.

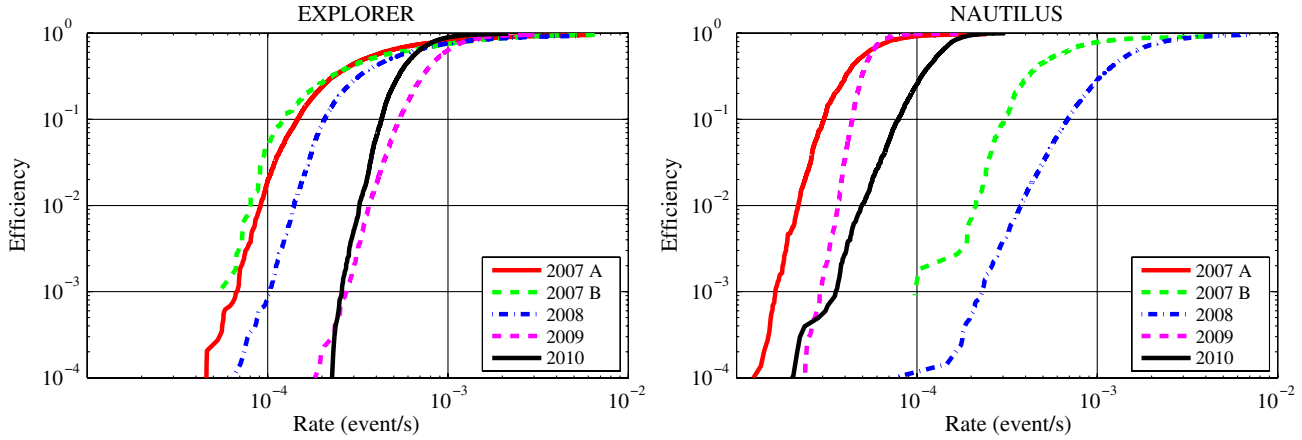

FIG. 5 (color online). ROCs for Explorer and Nautilus, at an injected amplitude $h_{\rm rss} = 9.76 \times 10^{-20}$ $s^{1/2}$ in the five subperiods.

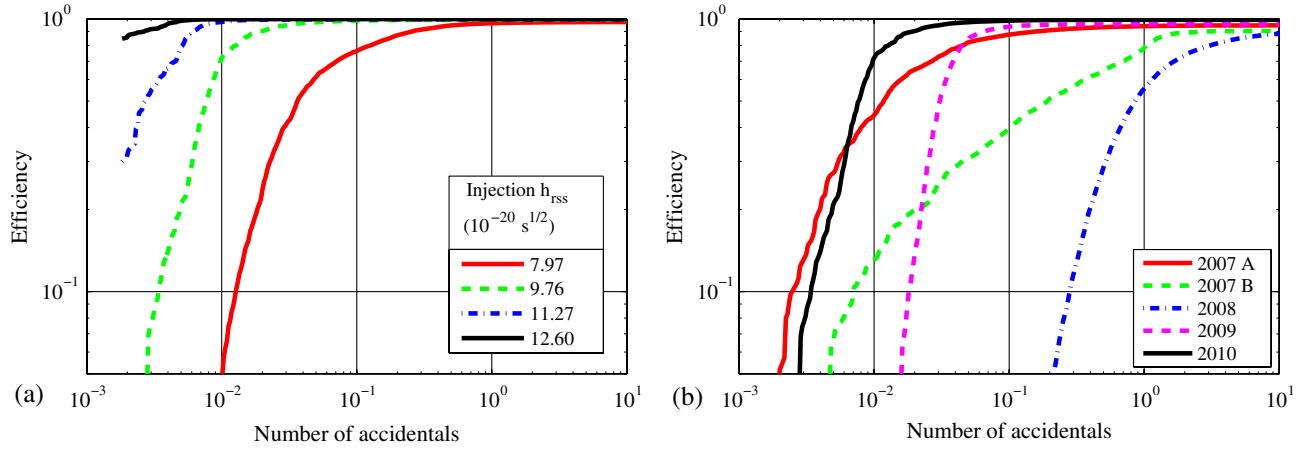

FIG. 6 (color online). ROCs for the combined observatory (Explorer + Nautilus). Left: in 2010, at the four injection amplitudes considered in Fig. 4; right: at an injected amplitude $h_{\rm rss} = 9.76 \times 10^{-20}$ $s^{1/2}$ in the five subperiods.

where we demand triple coincidences ($t_{\rm EX}$, $t_{\rm NA}$ and $t_{\rm inj}$), and in the set of shifted coincidences, for the accidentals.

(ii) In this way we create a M*M matrix with values of efficiency and accidentals for each threshold pair.

(iii) For each of N chosen values of accidentals, we search the matrix for those intervals that contain that value of accidentals. We interpolate in those intervals to find the value of thresholds and efficiency.

(iv) Finally, we compare these values and choose the one with the largest efficiency.

In our search, we used N = M = 100 and repeated the procedure for the 5 subperiods and for each of the 10 values of injected amplitudes.

Some of the ROCs for the observatory, obtained with this procedure, are shown in Fig. 6. Each point of these curves represents the threshold pair that produces the desired value of accidentals with the best possible efficiency. This procedure yields approximated values for the data points, as they are obtained via interpolation: for this reason, the search was later refined around the selected threshold values.

IV. COINCIDENCE SEARCH

In order to perform the true-time (on-source) search, we must decide upon a unique set of 5*2 thresholds to be applied to the 2 detectors in each of the 5 subperiods. This set must provide the desired number of total accidentals (0.1) while achieving the maximum possible efficiency for GW signals.

The ROCs for the coincidences, previously determined, specify, in each subperiod and for each injection amplitude, what are the thresholds capable of obtaining a given value of accidentals with the maximum possible efficiency. The next step is to find how to distribute the total number of accidentals between the different periods in order to maximize the total efficiency defined as

$$\bar{\varepsilon} = \sum_{i=1}^{5} \frac{\varepsilon_i T_i}{T}, \tag{1}$$

where ε_i, T_i are the efficiency and duration of the subperiods and $T = \sum_i T_i$ is the total observation time.

We remark that this procedure pins down a different set of thresholds for each considered injection amplitude. In Fig. 7, the data points show the results of this optimization: each data point is obtained with its own optimized set of 10 thresholds; we call this curve "composite efficiencies." However, as the coincidence search has to be performed only once, we need a strategy to select a unique set of thresholds. Figure 7 also shows three curves describing the efficiency at all amplitudes for three selected sets of thresholds, namely those optimized for $(7.97, 9.43, 11.96) \times 10^{-20}$ $s^{1/2}$. We make here no assumption on the amplitude distribution of the GW signals we search for; therefore we selected a threshold set that best approaches the curve of "composite efficiencies" at all amplitudes, and in particular at the smaller ones (that are, in such a search, the most probable).

Clearly, the set of thresholds chosen for $h_{\rm rss} = 9.43 \times 10^{-20}$ $s^{1/2}$ (values detailed in Table III) is the one that performs best and was therefore selected.

Tables III and IV show how the overall background was distributed and how the efficiency of detection at several signal amplitudes changed over the 5 subperiods of the search. We note that the optimization procedure automatically weights the subperiods according to the data quality, virtually "turning off," without any manual adjustment, the noisiest periods, i.e., 2007B and 2008: where we have a noisier detector, there we get little or no contribution to the coincidence search.

When we finally applied this set of thresholds to the on-time data, no coincident events were found, thus returning a null result.

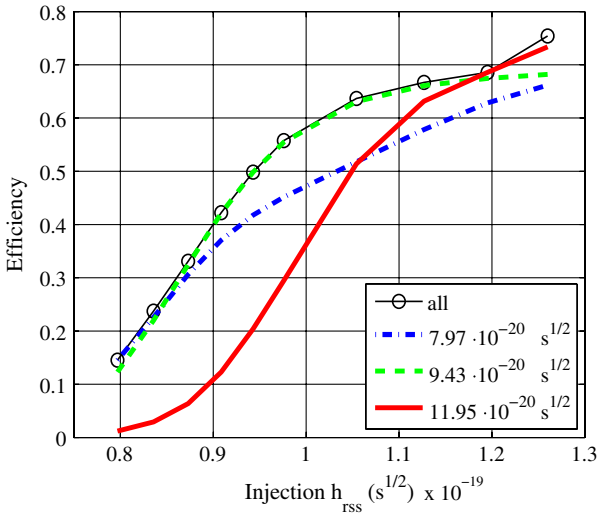

FIG. 7 (color online). Maximum efficiency $\bar{\varepsilon}$ achievable with a background set at 0.1 accidentals in the entire observation time. The top line shows the efficiency with thresholds optimized at each abscissa point (injected amplitude), while the other curves are produced with different choices of a unique set of thresholds.

TABLE III. The set of thresholds chosen for the final coincidence search and the resulting levels of accidentals in the five subperiods. These values are optimal for an injected signal with $h_{rss} = 9.43 \times 10^{-20}\, s^{1/2}$, but well approach the best possible efficiency at all signal amplitudes, as shown in Fig. 7. Note that 2007B gives no contribution to the accidental background.

Subperiod	$h_{rss}^{thr}[\cdot 10^{-20}\, s^{1/2}]$		Accidentals coincidences
	Expl	Naut	
#1: 2007 A	9.00	8.52	0.0206
#2: 2007 B	12.3	9.60	0.0
#3: 2008	10.8	19.3	0.0037
#4: 2009	8.12	8.17	0.0585
#5: 2010	8.19	8.29	0.0172

TABLE IV. Efficiencies at various amplitudes with the chosen set of thresholds (see Table III). Note that for 2008 the efficiency turns out to be zero at all amplitudes.

Injected h_{rss}	Efficiency in subperiod				
$[s^{1/2}] \times 10^{-20}$	2007 A	2007 B	2008	2009	2010
7.97	0.0935	0.0	0.0	0.2066	0.1520
8.36	0.1826	0.0018	0.0	0.3787	0.3162
8.73	0.2936	0.0018	0.0	0.5542	0.5137
9.09	0.4167	0.0036	0.0	0.7063	0.6856
9.43	0.5438	0.0100	0.0	0.8143	0.8081
9.76	0.6528	0.0190	0.0	0.8840	0.8869
10.54	0.8476	0.0805	0.0	0.9533	0.9712
11.27	0.9358	0.2081	0.0	0.9758	0.9920
11.95	0.9709	0.4009	0.0	0.9843	0.9963
12.60	0.9834	0.6091	0.0	0.9890	0.9980

V. UPPER LIMITS

A. Method

We now describe the procedure employed to compute the upper limits on the rate of incoming GW short bursts for a set of possible signal amplitudes: this procedure is separately applied to each of the 5 subperiods in which the entire observation time T was segmented. These results are then combined and an overall 95% bayesian upper limit is determined at each signal amplitude.

We remark that, when we compute the upper limit (UL) for a given GW amplitude, we are assuming the hypothesis that only signals of that very amplitude could reach the Earth. This means that each point in a UL curve is independent of any other point, and its determination can be independently optimized.

The handles we have for this optimization are, just as in the coincidence search previously described, the thresholds to be applied to the data: varying the thresholds allows us, in turn, to change:

(i) the background, i.e., the rate r_0, or the mean total number $\mu_0 = r_0 \cdot T$, of accidental coincidences.

These are, as before, estimated with the time-shifted data (Sec. III A).

(ii) the efficiencies ε, as computed with the software injections (Sec. III C).

The output of this search is the estimated maximum rate r of *incoming* GW signals, at any signal amplitude $h_{\rm rss}$ or, equivalently, the total number of *detected* GW signals $\mu = \varepsilon \cdot r \cdot T$. The optimization consists in choosing the thresholds potentially capable of producing the best, i.e., lowest, upper limit $r(h_{\rm rss})$.

We note that the optimization procedure is different from that employed in Sec. IV for the coincidence search: in that case we looked, at each amplitude, for the thresholds that would yield the best efficiency for a given (0.1 events) background of accidentals. Here, not being tied to a prefixed value of accidentals, we can choose the pair efficiency-background that optimizes our result.

B. The relative belief updating ratio *R*

The quantity we need to compute and optimize, for each value of assumed signal amplitude, is the *relative belief updating ratio* $\boldsymbol{R}$, i.e., the ratio of the likelihood $P(\mu_0 + \mu, N)$ that the N coincident events found be due to the presence of a given number μ of GW events, to the likelihood $P(\mu_0, N)$ of a mere accidental background.

By assuming, as usual, that the number N of coincidences found obeys the Poisson statistics, we then can write the likelihood in the presence of a rate r (corresponding to a detectable number μ) of GW events as

$$P(\mu_0 + \mu, N) = \frac{(\mu_0 + \mu)^N e^{-(\mu_0+\mu)}}{N!}. \tag{2}$$

The same relation, with $\mu = 0$, describes the likelihood $P(\mu_0, N)$ of mere background. Therefore, the relative belief updating ratio can be written, in terms of our parameters, as

$$\mathbf{R}(r) = \frac{(\mu_0 + \mu)^N e^{-\mu}}{\mu_0^N} = \left(1 + \frac{\varepsilon r}{r_0}\right)^N e^{-r\varepsilon} e^{-T}. \tag{3}$$

The determination of the maximum rate $r(h_{\rm rss})$ of GW, reaching the Earth with a given amplitude, requires the elaborate procedure outlined below. For sake of clarity, we describe it for a fixed value of $h_{\rm rss}$, implying that it is then repeated for all amplitudes of interest.

Requiring a 95% confidence limit means finding the particular value r^* such that $\mathbf{R}(r^*) = 0.05$. Equation (3) shows that $\boldsymbol{R}$ also depends on other parameters, so that an optimization is possible: we can vary our *handles* (i.e., the thresholds) until we find the minimum value among all r^*. The functional dependence of $\boldsymbol{R}$ on the thresholds is due to two competing effects: by raising the thresholds, we decrease both r_0 (that decreases $\boldsymbol{R}$) and ε, i.e., μ (that increases $\boldsymbol{R}$). The result cannot be analytically predicted, and a numerical search should be done by varying the thresholds. Actually, part of this work has already been done in computing the ROCs (see Sec. III D): we found there the optimal efficiency for each number (or rate) of accidentals. This simplifies our search: rather than probing the entire (r_0, ε) plane, we only need to compute $\mathbf{R}(r|r_0, \varepsilon)$ along the ROC curve corresponding to the $h_{\rm rss}$ considered, as in Fig. 6. We now have a family of curves $\boldsymbol{R}(r)$ depending on one parameter: the (r_0, ε) pair. Of all these curves, we select the one where the relation $\mathbf{R}(r^*) = 0.05$ is achieved with the lowest value r^*.

One last ingredient is missing for this calculation: the total number N of coincidences: it is provided by the "on-time" analysis that cannot be performed before setting all the search parameters. We have then implemented the following work around: for each pair (μ_0, ε) from the ROC, we solve for r^* the relation $\mathbf{R}(r^*) = 0.05$ at all possible values of $N_{\rm acc}$. We then compute the weighted average of these r's:

$$\bar{r}^* = \sum_{N_{\rm acc}} r^*(N_{\rm acc}) \cdot P(\mu_0, N_{\rm acc}). \tag{4}$$

In practice, the sum is truncated when

$$\sum_{N_{\rm acc}}^{M} P(\mu_0, N_{\rm acc}) \geq 1 - 1 \times 10^{-10}. \tag{5}$$

Finally, we choose the threshold pair that yields the minimum $\bar{r}^*$, i.e., that minimizes the expected UL based on our efficiency and accidental rate. The search is then repeated at a different value of GW amplitude, until the curve $r(h_{\rm rss})$ is traced.

The entire calculation is an "*a priori*" procedure, performed without any knowledge of the on time coincidences.

C. Upper limit evaluation

The above procedure was applied to find the optimal threshold pairs in the 5 time subperiods and for 19 different injection amplitudes [23]. Only at this point, we had the right to "open the box" and find the *on time* coincidences.

Figure 8 shows the thresholds for Explorer and Nautilus resulting from the UL optimization.

Figures 9(a) and 9(b) show, as an example, the $\boldsymbol{R}(r)$ curves at $h_{\rm rss}^{\rm inj} = 5.63 \times 10^{-20}$ and 7.97×10^{-20} $\rm s^{1/2}$ in the five subperiods, as well as the total $\boldsymbol{R}(r)$, obtained by multiplying the curves of all subperiods. In Figs. 10(a) and 10(b) we report the total $\boldsymbol{R}(r)$ computed at various $h_{\rm rss}^{\rm inj}$.

The standard procedure, at this point, calls for evaluation of the UL as the product of $\boldsymbol{R}(r)$ and a *prior*, containing all of our previous knowledge on ULs. The best prior is, in principle, a combination of all previously computed ULs (e.g., Refs. [3,4]). However, this cannot be used, due to different meanings and methods of these ULs, as discussed in the next section. We are then left with the choice of a purely theoretical *prior*: as we make no assumptions on the source location, polarization, sky distribution etc., it is

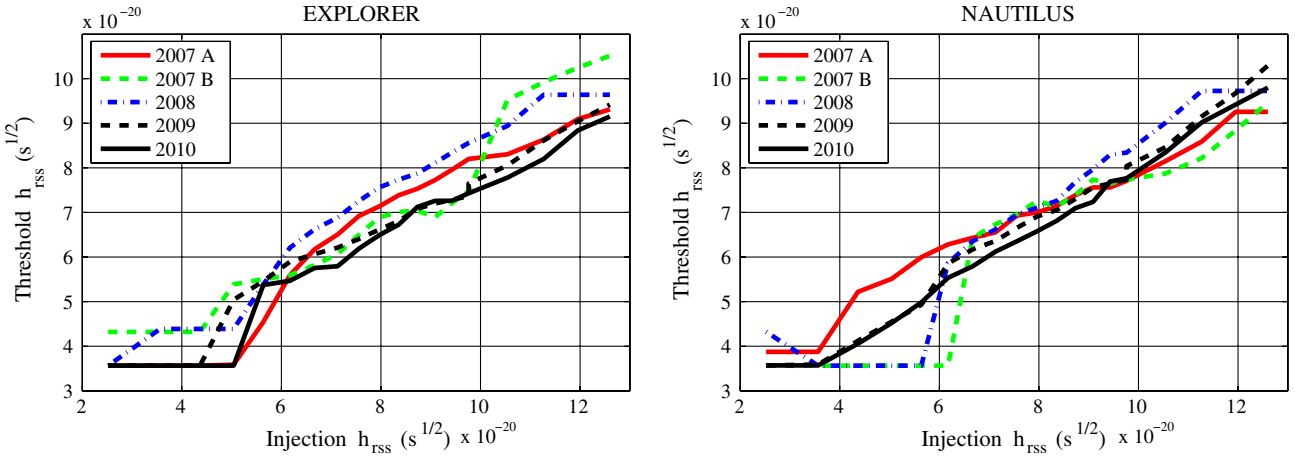

FIG. 8 (color online). Thresholds of Explorer and Nautilus resulting from the UL optimization.

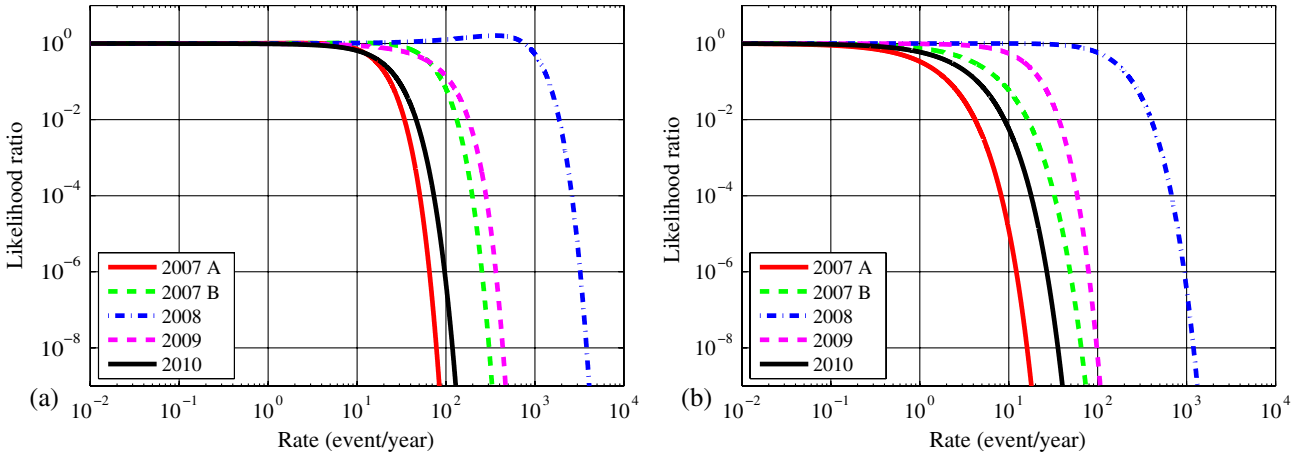

FIG. 9 (color online). ***R***-curves at $h_{\mathrm{rss}} = 5.63 \times 10^{-20}$ (a) and 7.97×10^{-20} (b) $\mathrm{s}^{1/2}$ in the five subperiods of data taking.

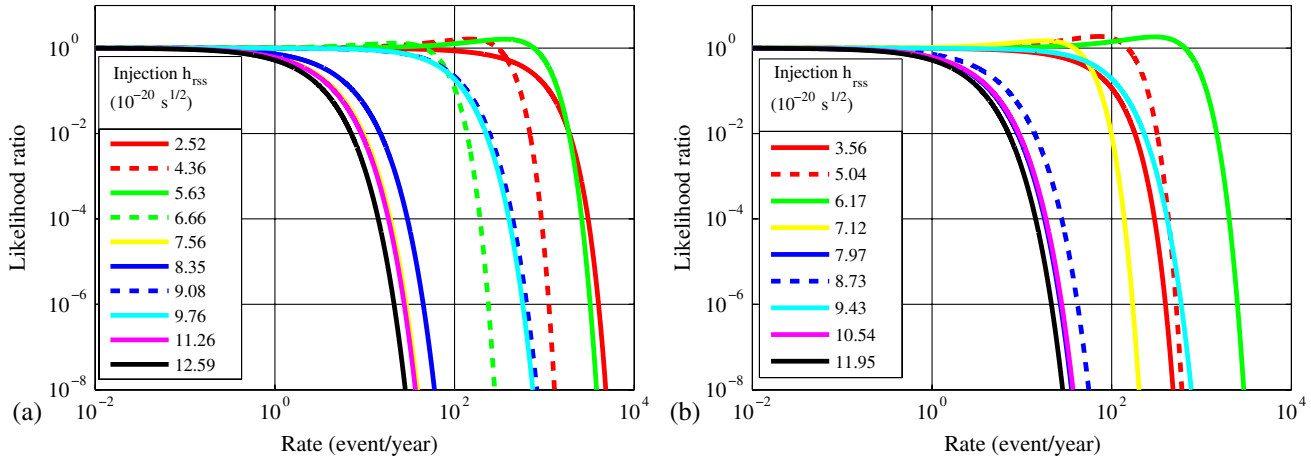

FIG. 10 (color online). Total ***R***-curves at different values of injected h_{rss}.

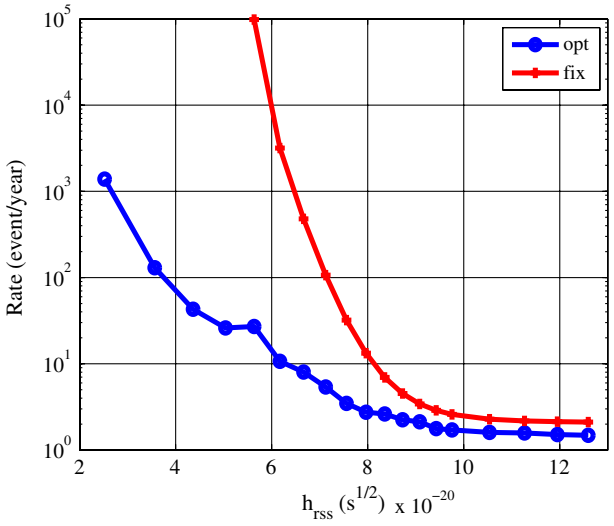

FIG. 11 (color online). Comparison between the upper limit computed with the optimized procedure described in the text (opt) and with a procedure with fixed thresholds, those defined by the coincidence search (fix). There is an evident large gain at low amplitude.

reasonable to assume a flat *prior*. Our 95% UL is then simply obtained by picking the value of r that yields $\boldsymbol{R} = 0.05$.

Figure 11 shows the *on time* results for the UL at different values of h_{rss}. The statistical uncertainties on the determination of efficiencies and accidentals (μ_0) causes on the evaluation of the ULs a relative error at 1σ ranging from 4% to 0.4% for h_{rss} going from the lowest to the highest value, respectively. The various parameters entering the final evaluation of the UL, namely the number of *on-time* coincidences N_{coi}, the estimated accidentals μ_0 and the computed efficiencies, are reported in Table V for all the values of injected h_{rss} and all five subperiods.

VI. DISCUSSION AND CONCLUSIONS

A. Comparison with other experiments

Figure 12 compares our present results with some other published in the past: the curve labeled "IGEC 1" is from Ref. [2], "IGEC 2" is from Ref. [3], "S2" is the UL for 1 ms gaussian pulses from the LIGO S2 run [24], "S4", "S5" and "LV2" are for Q = 9 sin-Gaussian pulses at 1053 Hz from Refs. [4,25,26].

In the present calculation of UL there are several choices that make it difficult to compare with previous results.

If we consider the above cited upper limits released by the LIGO Scientific Collaboration (LSC), we can see that no specific optimization was carried out for the UL: all the analysis parameters, and in particular the thresholds, were set for the coincidence search. The number of *on-time coincidences* found was directly used to compute the UL for that run. We show in Fig. 11 what the result of such an analysis strategy would be on our data: the curve labeled "opt" represents the optimized UL computed in the previous section while the curve labeled "fix" is the result we would obtain with the thresholds determined in the

TABLE V. Characteristic parameters computed in order to evaluate the $\boldsymbol{R}(r)$ curves in the 5 subperiods: N_{coi} is the *on time* number of coincidences detected, μ_0 is the estimated average background and ε is the efficiency of detection at each particular value of h_{rss}.

$[s^{1/2}] \times 10^{-20}$	2007 A			2007 B			2008			2009			2010		
h_{rss}	N_{coi}	μ_0	ε	N_{coi}	μ_0	ε	N_{coi}	μ_0	ε	N_{coi}	μ_0	ε	N_{coi}	μ_0	ε
2.52	565	553.9	.0245	66	63.04	.0179	639	663.2	.0159	283	303.4	.0193	94	103.2	.0161
3.56	565	553.9	.1396	66	63.04	.0868	638	663.2	.0910	273	295.5	.1909	94	103.2	.2227
4.36	95	85.67	.1432	66	63.04	.2139	638	663.2	.2272	109	130.8	.3536	40	45.68	.4378
5.04	57	48.94	.2532	32	23.92	.2612	638	663.2	.3784	30	37.01	.3699	18	24.30	.6078
5.63	20	18.74	.3090	26	21.31	.3864	390	408.2	.4192	15	15.95	.4611	5	3.856	.5261
6.17	5	7.177	.3600	25	19.89	.5002	111	97.72	.3133	1	3.208	.4180	2	1.536	.6222
6.67	2	3.588	.4339	7	6.881	.4406	46	41.23	.3354	1	1.457	.5283	1	.7959	.7130
7.13	1	2.162	.5288	5	4.439	.5068	30	25.37	.4041	0	.9320	.6522	1	.5365	.8032
7.56	0	.7643	.5472	3	2.930	.5518	19	12.93	.4341	0	.5226	.7189	0	.3088	.8393
7.97	0	.5404	.6346	2	1.890	.5836	8	8.396	.4946	0	.3342	.7762	0	.2028	.8728
8.36	0	.3344	.6941	1	1.935	.6806	7	6.411	.5696	0	.2437	.8347	0	.1403	.9019
8.73	0	.2242	.7465	1	1.646	.7292	3	4.395	.6091	0	.1643	.8606	0	.0749	.9031
9.09	0	.1503	.7892	1	1.401	.7623	2	3.095	.6403	0	.1297	.8899	0	.0589	.9289
9.43	0	.1063	.8281	1	1.369	.8166	0	2.122	.6620	0	.1079	.9126	0	.0477	.9497
9.76	0	.0712	.8526	1	1.248	.8491	0	1.805	.7164	0	.0787	.9217	0	.0387	.9650
10.54	0	.0491	.9257	0	.2660	.7679	0	1.024	.7810	0	.0545	.9548	0	.0223	.9834
11.27	0	.0296	.9537	0	.1186	.8439	0	.5361	.7897	0	.0387	.9652	0	.0135	.9892
11.95	0	.0140	.9647	0	.0594	.8952	0	.5361	.8967	0	.0305	.9755	0	.0084	.9919
12.60	0	.0113	.9790	0	.0265	.9210	0	.5361	.9455	0	.0254	.9821	0	.0068	.9959

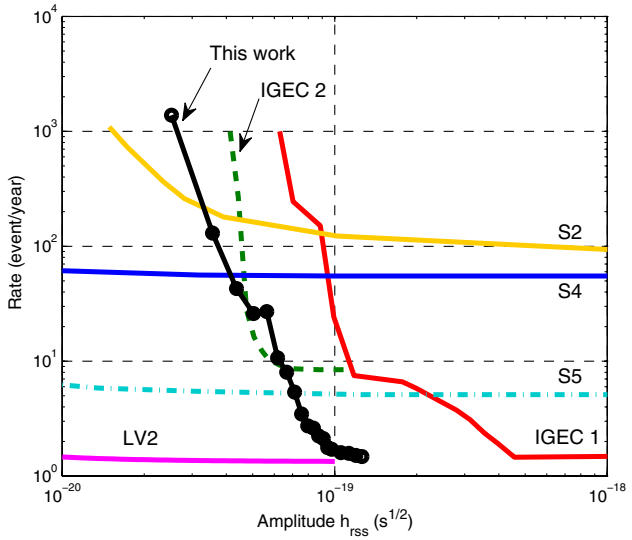

FIG. 12 (color online). Comparison between our 95% upper limit and previously published results. All LIGO and Virgo results, and in particular the solid curve (LV2), refer to 90% ULs.

coincidence search. The improvement in sensitivity, especially at low amplitudes can be clearly seen.

A more relevant issue regards the meaning of the variable $h_{\rm rss}$, i.e., the abscissa of the UL plot. In the two IGEC searches [2,3] the efficiency of the detectors was not considered, and the UL was plotted vs the amplitude threshold used in the coincidence search. What the curve really meant was then the UL on GW rates *detectable* by the observatory with that threshold, rather than the *incoming* rate. For a fair comparison, at least the efficiency of the detectors should be considered: for a given amplitude h_0, when the threshold is set at that very amplitude h_0, the efficiency is roughly $(1/2)^n$ where n is the number of detectors. The IGEC UL values should therefore be increased by at least a factor 4 to convert to an *incoming* rate.

On the other hand, the LSC includes in its analysis a model describing the distributions of the GW incoming signals, by folding into the calculation a factor $f(\theta, \phi) \leq 1$ to account for isotropic direction and random polarization of the wave. The $h_{\rm rss}$ in LIGO's UL is then the maximum amplitude detectable by the observatory. Besides, they computed a 90% UL, while ours is at 95%: according to Eq. 4.1 of Ref. [4], in order to convert their ULs at 95%, they should be increased by a factor $\simeq 1.3$. It is clear that the combination of these two differences, one of which would lead to a decrease of the UL, the other one to an increase, would anyhow not change much the comparison with our results.

B. Does the subperiod segmentation pay off?

It is reasonable to question whether a unique search over the entire observation period T would yield a similar or better result with respect to our choice of segmenting the analysis in 5 subperiods. In other terms, how does the global $\mathbf{R}_G(r)$ compare vs the product $\mathbf{R}_T(r) = \prod \mathbf{R}_i(r)$ of 5 separate update ratios? An exact answer can be given in the simple case where we segment T in two subperiods having the same characteristics, namely accidentals μ_0 and efficiency ε, assumed constant. In this case, the global (one period) $\boldsymbol{R}$ is given by Eq. (2), while the product of the two $\boldsymbol{R}$'s for the subperiods T_1, T_2 is

$$\mathbf{R}_T(r) = \prod_{i=1}^{2} \frac{(\mu_i + \mu_{0,i})^{N_i} e^{-\mu_i}}{\mu_{0,i}^{N_i}}. \tag{6}$$

As $\mu_0 = \mu_{0,1} + \mu_{0,2}$ (and same for μ) and $N = N_1 + N_2$, one can expand Eq. (6), and prove $\boldsymbol{R}_T \equiv \boldsymbol{R}_G$, for any choice of T_1, T_2, N_1, N_2.

For the more general case of two nonhomogeneous subperiods, although we lack an algebraic proof, extensive numerical investigation has shown that we should always expect $\boldsymbol{R}_T < \boldsymbol{R}_G$.

C. Conclusions

In this paper we analyzed 3 years of almost continuous data from the two resonant gravitational wave detectors Explorer and Nautilus. The period examined spans from the end of the IGEC2 four-detector analysis to the decommissioning of Explorer. Both the search for coincidences with low false alarm rate and the evaluation of the upper limit have been performed employing a novel type of analysis, with optimization of the thresholds of each detector separately for each intermediate task. This method has proven successful in obtaining better results (see for instance Fig. 11) as well as for handling nonstationarities in the detectors' behaviors. As an example, we recall the noisy period of 2007B: in a search with the usual procedure, that period would be discarded, or its large number of events would negatively affect the statistics of the remaining, better data. In our case, the optimized procedure automatically takes care of the higher noise and reduces the weight of that period on the final results. Indeed, its contribution to both the coincidence search and the upper limit evaluation is hardly noticeable.

The upper limit computed on the basis of our data cannot compete with those of the more sensitive interferometric detectors, that extend down to much smaller $h_{\rm rss}$ values. Nevertheless, the length of our data collection led us to expect that we could improve upon the UL set by LIGO S5, at amplitudes of the order of $h_{\rm rss} \sim 10^{-19}$ $\mathrm{s}^{1/2}$: indeed we did obtain a better UL than other previously published. However, while in the process of analyzing our data, a new, improved UL was released by the LSC-VIRGO collaboration: combining the data of the S5/VSR1 and S6/VSR2-3 runs, the extended data taking allowed them to set a better limit also at higher amplitudes.

The procedure detailed here could be profitably used in future searches, where better sensitivity of the detectors would yield even more significant ULs. In fact, we demonstrated (see Fig. 11) that this procedure grants a

substantial improvement in the evaluation of the upper limit, up to two orders of magnitude at low amplitudes, with respect to the standard way of computing it.

ACKNOWLEDGMENTS

Explorer ceased taking data on June 11, 2010, concluding an activity that spanned over a quarter of a century. We take the opportunity of this paper produced with its last data to thank CERN as an institution for hospitality and provision of facilities, first and foremost the cryogenic fluids. We also thank the numerous CERN officials and staff that provided, over such a long period, with logistics and with daily as well as emergency help. We are grateful to the technicians (too numerous to name them all) that, over the years, helped us maintain both detectors in operations and, to these days, still work to keep Nautilus on the air.

[1] Z. A. Allen *et al.*, Phys. Rev. Lett. **85**, 5046 (2000).
[2] P. Astone *et al.*, Phys. Rev. D **68**, 022001 (2003).
[3] P. Astone *et al.*, Phys. Rev. D **76**, 102001 (2007).
[4] See, for instance, J. Abadie *et al.*, Phys. Rev. D **85**, 082002 (2012).
[5] E. Amaldi *et al.*, Nuovo Cimento Soc. Ital. Fis. **7C**, 338 (1984).
[6] P. Astone *et al.*, Phys. Rev. D **47**, 362 (1993).
[7] P. Astone *et al.*, Phys. Rev. Lett. **91**, 111101 (2003).
[8] P. Astone *et al.*, Europhys. Lett. **16**, 231 (1991).
[9] P. Astone *et al.*, Astropart. Phys. **7**, 231 (1997).
[10] P. Astone *et al.*, Classical Quantum Gravity **19**, 5449 (2002).
[11] P. Astone *et al.*, Classical Quantum Gravity **23**, S169 (2006).
[12] P. Astone *et al.*, Phys. Lett. B **385**, 421 (1996).
[13] J. Zendri *et al.*, Classical Quantum Gravity **19**, 1925 (2002).
[14] M. P. McHugh, W. W. Johnson, W. O. Hamilton, J. Hanson, I. S. Heng, D. McNeese, P. Miller, D. Nettles, J. Weaver, and P. Zhang, Classical Quantum Gravity **22**, S965 (2005).
[15] E. Coccia, A. Marini, G. Mazzitelli, G. Modestino, F. Ricci, F. Ronga, and L. Votano, Nucl. Instrum. Methods Phys. Res., Sect. A **355**, 624 (1995).
[16] P. Astone *et al.*, Phys. Rev. Lett. **84**, 14 (2000).
[17] P. Astone *et al.*, Astropart. Phys. **30**, 200 (2008).
[18] P. Astone *et al.*, Phys. Lett. B **499**, 16 (2001).
[19] M. Bassan *et al.*, Nucl. Instrum. Methods Phys. Res., Sect. A **659**, 289 (2011).
[20] P. Astone *et al.*, Phys. Rev. D **82**, 022003 (2010).
[21] Traditionally, the GW resonant detectors community indicates the antenna sensitivity, i.e., the long term quadratic average of $h(t)$, in terms of a "detection noise temperature" $T_{\rm eff}$. These two quantities are related, for our detectors, by $\langle h^2 \rangle = 6.35 \times 10^{-35} T_{\rm eff}$. In these units, the average noise levels of Table I spanned between 0.9 and 4 mK.
[22] P. Astone *et al.*, Classical Quantum Gravity **23**, S57 (2006).
[23] Beside the 10 values of injected amplitude used in the coincidence search, we also explored the small signal region repeating the injection at 9 additional amplitudes in the range $[2.52 \div 7.56] \times 10^{-20}$ $s^{1/2}$.
[24] B. Abbott *et al.*, Phys. Rev. D **72**, 062001 (2005).
[25] B. Abbott *et al.*, Classical Quantum Gravity **24**, 5343 (2007).
[26] B. Abbott *et al.*, Phys. Rev. D **80**, 102002 (2009).